Fabrication and Characterization of Femtosecond Laser Inscribed Long-Period Fiber Grating in Few-Mode Fiber

Jing Liu, Cailong Yang, Zhiyong Zhao, Deming Liu, and Ming Tang

***Abstract*—We experimentally investigated the fabrication and characterization of long-period fiber grating in few-mode fiber (FMF-LPFGs) by using the femtosecond laser direct writing technique. Thanks to the high flexibility and repeatability of this technique, stable FMF-LPFGs fabrication technology has been developed. In addition, the properties of FMF-LPFGs have also been characterized. The coupling of LP_{01}- LP_{11} and LP_{01}- cladding mode LP_{13} were investigated by both the transmission spectrum and the mode patterns. The temperature, strain and twist sensitivities of the resonance dips were calibrated by experiments, and the sensitivity difference between the dips was explained. By using their disparate responses to external temperature and strain, a cross coefficient matrix was established and dual-parameter discrimination determination is realized. This work provides a thoroughly theoretical and experimental investigation on the fabrication and characterization of FMF-LPFGs based on femtosecond laser direct writing technique. It is believed that the flexible and efficient LPFGs fabrication technique will benefit a lot in the future for developing various functional specialty optical fiber devices and sensors.**

***Index Terms*—Femtosecond laser direct writing, long period fiber grating, few-mode fiber, optical fiber sensors.**

I. Introduction

With the increasing demand for ultra-high capacity data transmission, mode division multiplexing (MDM) based on few-mode fiber (FMF) is proposed as a promising way to boost the transmission capacity [1]. On the other hand, FMFs have also found good applicability for sensing application, which possesses some advantages in comparison with the traditional single-mode fiber (SMF) based sensors by using its multi-spatial modes. As one of the most common FMF devices, FMF long-period fiber gratings (FMF-LPFGs) has been widely investigated, e.g., serves as the passive mode coupler, which has the advantages of low cost, low insertion loss, flexible structure, easy integration and high mode coupling efficiency [2]. In addition, FMF-LPFGs based sensors have the prominent merit of allowing for multi-parameter discriminative measurements by utilizing multiple resonant dips that are generated by coupling from fundamental modes to high order core modes and cladding modes, respectively.

So far, several FMF-LPFGs fabrication techniques have been developed, including the UV laser exposure [3], CO_2 laser irradiation [4], mechanical micro-bending [5] and micro-taper based method [6], etc. However, the traditional UV laser exposure technique requires a time-consuming pretreatment procedure such as hydrogen loading to enhance the photo-sensitivity of fiber. In addition, the requirement of phase or amplitude masks also limits the flexibility of this method. The CO_2 laser irradiation technique has better fabrication efficiency and higher thermal stability [7], [8]. Nonetheless, its disadvantages of high polarization-dependent loss (PDL) and low uniformity restrict the possibility of large-scale application. The mechanical micro-bending and micro-taper based methods have lower repeatability and mechanical stability owing to their damage on fiber structure. Femtosecond laser is a powerful tool for fabricating various functional devices by generating permanent refractive index changes inside transparent optical materials including single crystals, bulk glasses, optical fibers, or semiconductor chips [9], etc. Due to the ultra-short pulse duration and ultra-high peak intensity of femtosecond laser pulse [10], the nonlinear property of its absorption process gives rise to highly localized refractive index (RI) profiles without damaging the surrounding material [11]–[14]. Compared with these fabrication methods, the femtosecond (fs) laser direct writing technique has the advantages of low PDL, high flexibility and repeatability. However, a systematic investigation on the fabrication and characterization of FMF-LPFGs using fs laser inscription technique is rarely reported by now.

In this work, stable FMF-LPFGs were fabricated by using the fs laser direct writing technique, where two resonant dips can be observed in the transmission spectrum. The properties of FMF-LPFGs have been characterized, and the mode coupling mechanism of two resonant dips were investigated respectively with the assistance of the transmission spectrum and mode patterns. The simultaneous mode conversion from fundamental mode

Manuscript received April 13, 2022; revised May 10, 2022; accepted May 15, 2022. Date of publication May 20, 2022; date of current version June 7, 2022. This work was supported in part by the National Key Research and Development Program of China under Grant 2021YFB2800902, in part by the National Natural Science Foundation of China under Grants 61931010 and 62105111, in part by the Fundamental Research Funds for the Central Universities under Grant HUST: 2021XXJS026, in part by the Hubei Province Key Research and Development Program under Grant 2021BAA008, and in part by the Natural Science Foundation of Hubei Province under Grant 2021CFB049. *(Corresponding author: Zhiyong Zhao.)*

The authors are with the Wuhan National Lab for Optoelectronics, School of Optical and Electronic Information, Huazhong University of Science and Technology, Wuhan 430074, China (e-mail: elmeroii@163.com; yangcailong@hust.edu.cn; zhiyongzhao@hust.edu.cn; dmliu@mail.hust.edu.cn; tangming@mail.hust.edu.cn).

Digital Object Identifier 10.1109/JPHOT.2022.3176009

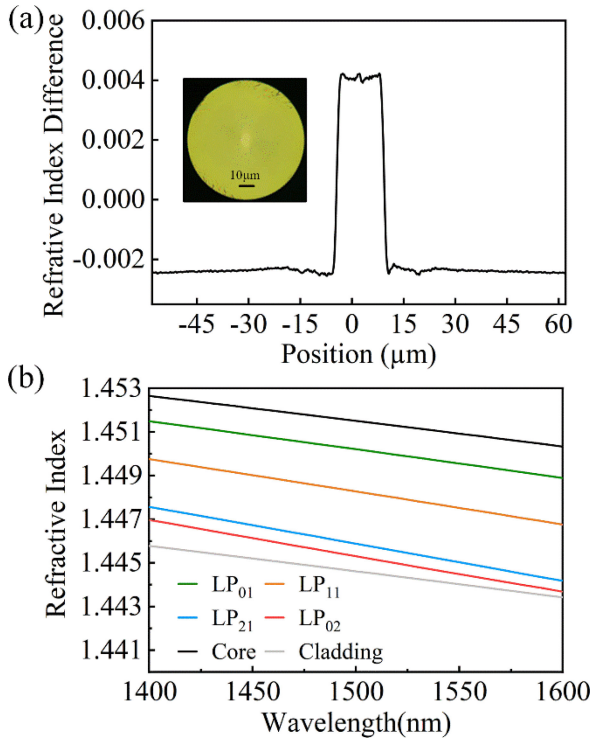

Fig. 1. (a) Measured refractive index profile of the FMF. (b). The effective refractive index of guided modes with respect to wavelength.

to core mode LP_{11} and high-order cladding mode LP_{13} over 1500–1550 nm band is successfully achieved. To investigate the responses of resonant dips to common external disturbances in practical application scenarios, we measured the sensitivities of temperature, strain, and twist of the FMF-LPFGs, and a theoretical analysis was carried out to explain the difference in sensitivity between these two dips. By making use of the different responses to temperature and strain, a cross coefficient matrix is established and dual-parameter discrimination determination was experimentally demonstrated.

II. Fabrication and Properties of FMF-LPFGs

A few-mode fiber with a step-index profile was used in the experiments. Fig. 1(a) shows the refractive index profile and the end view of the FMF. The core radii are 7.6 μm and the cladding radii are 62.5 μm, respectively. Besides, the refractive index (RI) of fiber core and cladding are 1.4506 and 1.444 at 1550 nm, respectively. Then we calculated the effective RI of the guided modes arising in the FMF by simulation based on the finite-element method, and the calculated effective refractive indexes of the linear polarization modes LP_{01}, LP_{11}, LP_{21} and LP_{02} as a function of wavelength are shown in Fig. 1(b).

The experimental setup used for LPFGs writing is schematically illustrated in Fig. 2. The femtosecond laser (Satsuma, Amplitude System) operates at 1030 nm, generating pulses of 270 fs duration, and the repetition rate ranges from 0 kHz to 250 kHz. The laser pulse is focused into the few-mode fiber with a 20 $\times$ objective lens (NA = 0.5, Olympus UPlanFl), after being

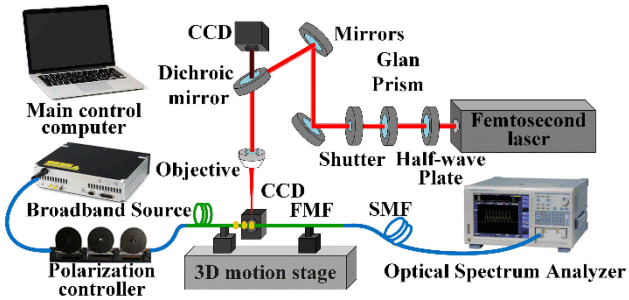

Fig. 2. The fabrication platform setup of the FMF-LPFGs.

attenuated by a combination of half wave-plate and Glan prism. An Optical shutter is used to control the laser irradiation time. The FMF is placed on a three-dimension motion stage (XMS, Newport) with 50 nm theoretical motion resolution. Real-time monitoring is realized by using the horizontal and vertical double CCDs to adjust the alignment of fiber. Light from the supercontinuum optical source (SCS, YSL Photonics) is launched into the FMF after a polarization controller (PC), and an optical spectrum analyzer is used to trace the transmission spectrum with a resolution of 0.02 nm for real-time characterization of the LPFGs writing.

During the writing process, the average pulse energy after the attenuator was set at 13.3 mW and the used repetition rate was 10 kHz. The LPFGs were inscribed point-by-point with the Y-axis scanning direct writing technique [15]. The FMF placed on the motion stage moved along a pre-planned route. At each point, the laser beam was focused at the center of the fiber core, then the stage moved to scan along the fiber radius direction to enhance the mode coupling strength by modulating a larger volume [16]. While light may leak out from the machined boundary between the fiber core and cladding, as a result the insertion loss may be increased. This problem can be mitigated by compensating the aberration and optimizing the cooperation between the 3D motion stage t and the optical shutter to reduce the volume of modulated cladding region. The axial grating period was set at 776 μm. Fig. 3(a) shows the transmission spectrum of the fabricated LPFGs. It is observed that, with the increment of the inscribed periodic points, the resonant dips go deeper and the resonate wavelength shifts towards the longer wavelength region [17], until complete coupling. The polarization dependence of the fabricated FMF-LPFGs was investigated, and the maximum polarization induced loss, which is defined as the intensity change of two resonant dips caused by changing the polarization state of the incident light through a polarization controller, reached 3.5 dB, as shown in Fig. 3(b). The polarization induced loss is caused by the asymmetry of the RI modified area. Thanks to the Y-axis scanning direct writing technique, the mode coupling strength is enhanced, as a result it will allow for shorter axial irradiated length than the conventional scheme [16], which helps to mitigate the scattering loss. Finally, the fabricated LPFGs achieves a maximum contrast of 10 dB and insertion loss of 3dB. It is worth mentioning that the quality of FMF-LPFGs can be further improved by optimizing

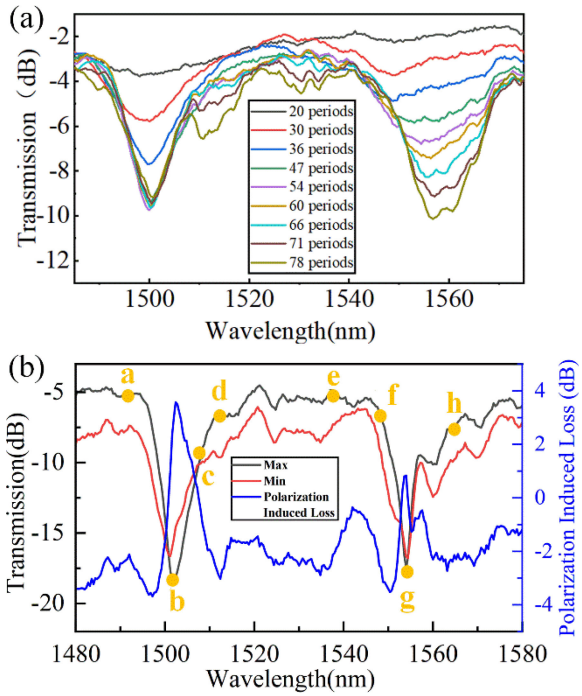

Fig. 3. (a) Evolution of the LPFGs transmission spectrum versus the scanning periods (b) the measured polarization induced loss.

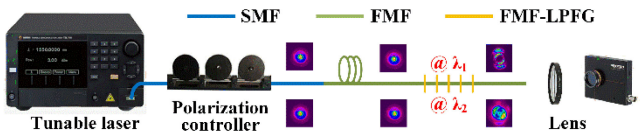

Fig. 4. Experimental characterization setup of FMF-LPFGs.

the laser power and performing aberration compensation in our fabrication system.

III. Characterization of FMF-LPFGs

In order to investigate the generation mechanism of the resonant dips of the transmission spectrum, mode coupling has been characterized by injecting light with different wavelengths and then observing the output mode patterns using a CCD, as shown in Fig. 4. The light from a tunable laser (TSL- 44710, Santec) was launched into the FMF with LPFGs inscribed. A polarization controller was placed between the tunable laser and the LPFGs to manage the polarization state of the input light. The mode field distribution after the LPFGs was captured by a collimation lens and a CCD (SP620U-1550, OPHIR Photonics). Fig.5 shows the measured mode patterns of the LPFGs output, where the period of LPFGs is 776 um. For each dip, four wavelengths covering their rejection band have been selected to observe the whole conversion process, and those eight wavelengths are also marked with labels from "a" to "h" in Fig. 3(b).

The resonant dips of LPFGs are formed by the coupling between the forward-propagating fundamental core mode and co-propagating cladding modes or high-order core modes. Its resonant wavelength λ_{res} was determined by the phase-matching

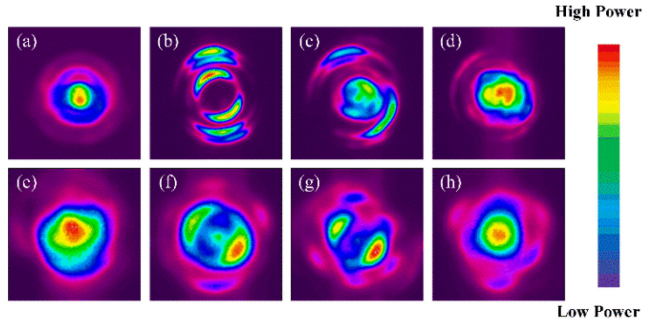

Fig. 5. Near-field intensity profile of the FMF output measured with eight different wavelengths (a)–(h) covering the resonant notch of LPFGs in Fig. 3(b).

condition [17]:

$$\lambda_{\mathrm{res}} = \left(n_{\mathrm{F}}^{\mathrm{eff}} - n_{\mathrm{H}}^{\mathrm{eff}}\right)\Lambda \tag{1}$$

where n_F^{eff} is the effective index of fundamental mode and n_H^{eff} is the effective index of the coupling mode, Λ is the grating period. Generally, LPFGs formed by circularly symmetric refractive index change of fiber allows the coupling between fundamental mode and circularly symmetric cladding mode $\mathrm{LP}_{0\mathrm{m}}$. However, when the input light wavelength is finely tuned near the resonant wavelength range of dip1, it is observed that the fundamental mode in Fig. 5(a) couples to the circularly asymmetric cladding mode LP_{13}, as shown in Fig. 5(b). This is attributed to the fact that the cladding RI is also modulated by fs laser due to the Y-axis scanning direct writing technique, resulting in the coupling of the circularly symmetric core mode and circularly asymmetric cladding modes [18]. Fig. 5(e)–(h) are the captured output mode patterns when the input wavelength is tuned across the resonant wavelength range of dip 2, which reveals a transition process from the LP_{01} mode to the LP_{11} mode and then going out of coupling. Therefore, it indicates that dip 2 is generated by the coupling between the fundamental mode LP_{01} and the LP_{11} mode. It is worth mentioning that the theoretical grating period that couples the two core modes is 770 μm according to Eq.(1). The error is considered to be caused by the inaccurate moving stage and the large size of the laser focus.

In practical deployment scenarios, external environmental change could affect directly the light coupling between different modes, which manifests in the shift of resonant wavelength. Therefore, the temperature, strain and twist responses of the resonance dips have also been calibrated by experiments. Each sensing experiment was repeated five times to ensure the repeatability of results and the stability of the sensor performance.

The experimental setup used for temperature and strain calibration is shown in Fig. 6, which allows for simultaneous measurement of both temperature and strain. Both ends of the FMF are fixed by a pair of fiber clamps with an initial interval of 19 cm. The axial strain applied to the fiber is controlled by the translation stages. Meanwhile, the whole part of FMF-LPFGs is placed on the thermoelectric cooler (TEC) with a resolution of 0.1 °C to change the external temperature. An external thermometer was used to calibrate the temperature of the TEC to avoid errors. Broadband light from a supercontinuum source

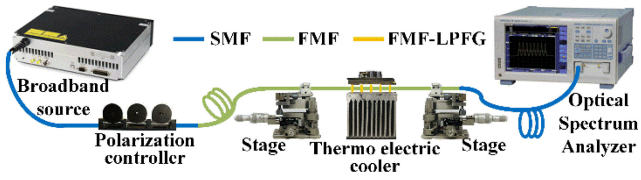

Fig. 6. Experimental setup for temperature and strain measurement.

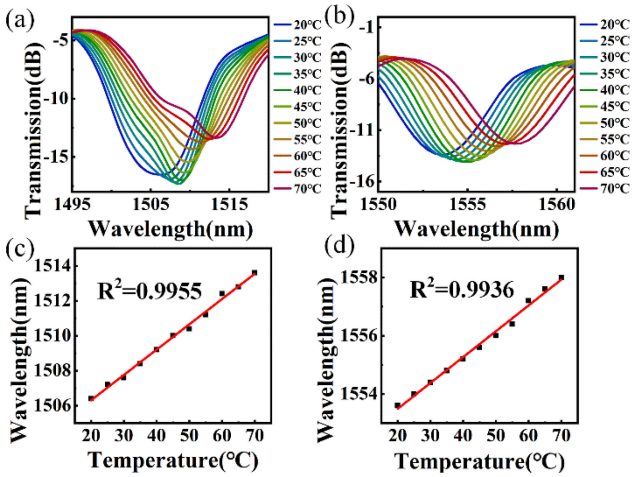

Fig. 7. Temperature response of transmission spectra are shown on (a) dip1, and (b) dip2. The corresponding wavelength shifts as a function of temperature are shown on (c) dip1, and (d) dip2.

was launched into the FMF-LPFGs after passing through a polarization controller, and the evolution of the output spectrum is monitored with an OSA. The polarization controller is used to eliminate the effect on the initial transmission spectrum caused by the change of polarization state during the placement of the grating.

To calibrate the temperature response of the FMF-LPFGs, the temperature of TEC is increased from 20 °C to 70 °C with a step of 5 °C. The transmission spectra of each step were stabilized for 20 minutes to ensure the establishment of temperature change. Fig. 7(a) and (b), show the wavelength shift of dip 1 and dip 2 respectively. With the increase of temperature, the resonant wavelengths of dip 1 and dip 2 are all linearly red-shifted. The R-square values of the linear fitting are 0.9955 and 0.9936, respectively. The temperature sensitivities of dip1 and dip2 are 144.7 pm/°C and 88.7 pm/°C, respectively. The standard deviations of the measured temperature sensitivities are 3.79 pm/°C and 1.34 pm/°C for dip1 and dip2. The analytic expression for the temperature sensitivity $d\lambda_{\rm res}/dT$ of the resonant wavelength is given by [19]:

$$\frac{d\lambda_{\rm res}}{dT} = \lambda_{\rm res} \cdot \gamma \cdot (\alpha + \Gamma_{\rm temp}) \tag{2}$$

where α is the thermal expansion coefficient of the fiber, γ describes the waveguide dispersion and it is defined by:

$$\gamma = \frac{\frac{d\lambda_{\rm res}}{d\Lambda}}{n_F^{\rm eff} - n_H^{\rm eff}} \tag{3}$$

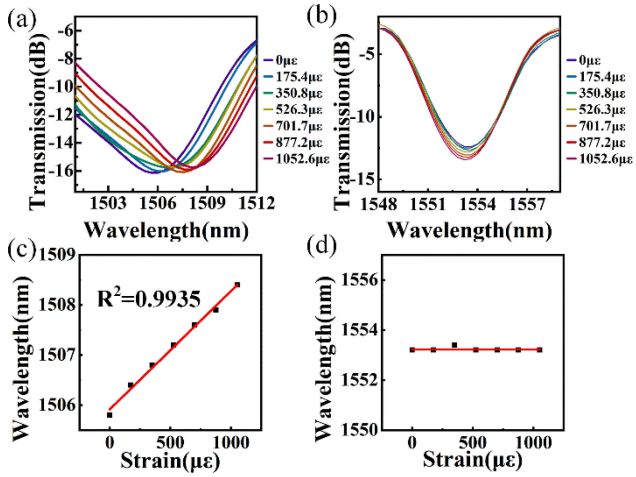

Fig. 8. Strain response of transmission spectra are shown on (a) dip1, and (b) dip2. The corresponding wavelength shifts as a function of strain are shown on (c) dip1, and (d) dip2.

$\Gamma_{\rm temp}$ is the temperature and strain dependences of the waveguide dispersion respectively, which can be defined as Eq. (4):

$$\Gamma_{\rm temp} = \frac{\xi_F n_F^{\rm eff} - \xi_{\rm H} n_H^{\rm eff}}{n_F^{\rm eff} - n_H^{\rm eff}} \tag{4}$$

$\xi_{\rm F}$, $\xi_{\rm H}$ are the thermo-optic coefficients of the core material and the material of waveguide where coupling occurs. Eq. (2) indicates that the temperature sensitivity of the resonant wavelength is mainly determined by the thermal expansion effect and the thermal-optic effect. The thermal expansion effect of LPFGs changes the volume of modulation area, which causes the change of the grating period. The effect of thermal-optic is mainly caused by the change of the effective refractive index of core mode and cladding mode.

In addition, the spectrum characteristics of LPFGs as a function of strain change have also been measured when the temperature is fixed at 20 °C. The axial strain varies from 0 $\mu\varepsilon$ to 1052.6 $\mu\varepsilon$ with a step of 175.4 $\mu\varepsilon$. For dip1, its resonant wavelength shifts to a longer wavelength with the increase of axial strain. The strain sensitivity of dip1 is 2.4 pm/$\mu\varepsilon$ and its linear fitting rate of R-square is 0.9935. The standard deviation of the measured strain sensitivity is 0.25 pm/$\mu\varepsilon$ for dip1. However, the resonant wavelength of dip2 turns out to be insensitive to strain, as shown in Fig. 8(b). Eq. (5) gives the formula of the strain sensitivity $d\lambda_{\rm res}/d\varepsilon$ [19].

$$\frac{d\lambda_{\rm res}}{d\varepsilon} = \lambda_{\rm res} \cdot \gamma \cdot (1 + \Gamma_{\rm strain}) \tag{5}$$

The strain dependence of the waveguide dispersion $\Gamma_{\rm strain}$ can be defined as:

$$\Gamma_{\rm strain} = \frac{\eta_F n_F^{\rm eff} - \eta_H n_H^{\rm eff}}{n_F^{\rm eff} - n_H^{\rm eff}} \tag{6}$$

where $\eta_{\rm F}$, $\eta_{\rm H}$ are the elastic-optic coefficients of the core material and the material of waveguide where coupling occurs. Dip 2 is generated by the fundamental mode LP_{01} coupled to the

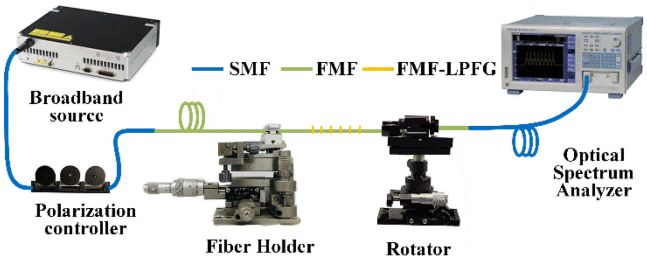

Fig. 9. Experimental setup for twist measurement.

LP_{11} mode. Hence the strain sensitivity $d\lambda_{\rm res}/d\varepsilon$ are determined by the core material. Since LP_{01} and LP_{11} are all core modes, we have $\Gamma_{\rm strain} = \eta_F$. This indicates that the strain sensitivity is completely decided by the elastic-optic coefficients of core material [6]. Because these two modes exist in the fiber core thus they have similar elastic-optic coefficients and strain sensitivity. As a result, dip2 shows insensitive to external strain. However, since the core material and cladding material have different elastic-optic coefficients, therefore dip1 which is generated by the coupling between the core mode and cladding mode turns out to be sensitive to strain change.

Furthermore, the response of fiber twist of the LPFGs has also been measured, and the used experimental setup is shown in Fig. 9. A supercontinuum source and an optical spectrum analyzer are connected with the LPFGs sensor to ensure real-time monitoring of the transmission spectrum. During the experiment, one end of the LPFGs is fixed to a stationary holder, and the other end is fixed to a fiber rotator. The distance between the fiber holder and the rotator is 15 cm. During the measurement, the grating is slightly strained to keep it straight for eliminating the unwanted fiber bending.

The effect of fiber twisting on the spectrum of the LPFGs was investigated experimentally. The transmission spectra of the LPFGs were recorded by increasing the twist angle from –180 to 180° with a step of 30°. Fig. 10(a) and (b) show the spectral evolution of the grating under twist. Fig. 10(a) shows that the resonant wavelength of dip 1 shifts randomly within a small wavelength range, which could be considered insensitive to twist. This might be caused by the appearance and disappearance of different cladding modes that contribute to the coupling when twist is applied. During the fs laser direct inscription process, the laser beam was scanned along the Y-axis at each inscription region to increase the modulating volume, which brings the asymmetry of modulating area. When twist is applied to LPFGs, there will be a fixed-angle rotation between each adjacent modulation region. Hence extra refractive index modulation might be generated, which causes the appearance and disappearance of modes that have different twist sensitivities. As a result, the wavelength shifts of different modes counteract with each other, and eventually dip1 turns out to be insensitivity to twist. It can be seen from Fig. 10(b) that with the increasement of twist, the resonant wavelengths of dip 2 are linearly red-shifted, which indicates that the LPFGs can be developed as a wavelength-interrogated twist sensor. Furthermore, the direction of twist could be distinguished based on the

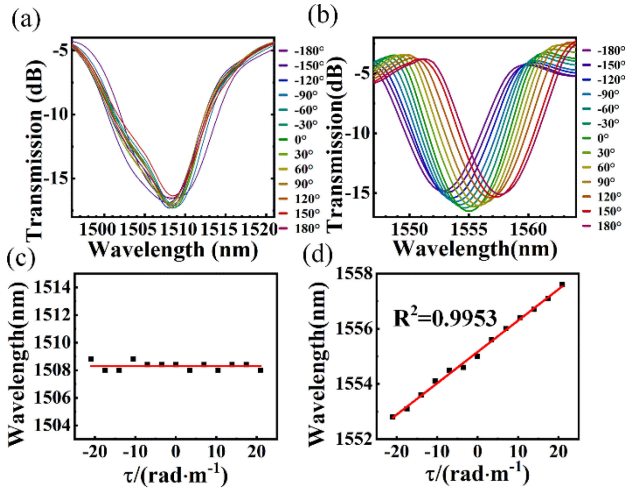

Fig. 10. Twist response of transmission spectra are shown on (a) dip1, and (b) dip2. The corresponding wavelength shifts as a function of strain are shown on (c) dip1, and (d) dip2.

TABLE I
DISCRIMINATIVE TEMPERATURE AND STRAIN MEASUREMENT

Actual value		Measured Value		Relative measurement error[a]	
Temperature(°C)	Strain(με)	Temperature(°C)	Strain(με)	Temperature	Strain
25	175.44	25.64	167.13	2.50%	4.73%
25	701.75	25.52	682.52	2.09%	2.74%
45	175.44	45.92	181.53	2.05%	3.47%
45	701.75	45.02	677.50	0.04%	3.46%
65	175.44	65.08	171.82	0.12%	2.06%
65	701.75	64.97	678.72	0.05%	3.28%

[a]Relative measurement error = $|\mathrm{T}' - \mathrm{T}|/\mathrm{T} \times 100\%$ or $|\mathrm{S}' - \mathrm{S}|/\mathrm{S} \times 100\%$

original resonant wavelength, since different twist direction will give rise to opposite wavelength shift direction. According to the linear fitting, dip 2 has a twist sensitivity of 0.013333 nm/deg (0.114592 nm/rad·m^{-1}), which is twice the twist sensitivity of regular SMF-LPFGs [20]. The standard deviation of the measured twist sensitivity is 0.00931 nm/rad·m^{-1} for dip2.

Since the two resonant dips have different temperature and strain sensitivities, this feature can be used to develop a LPFGs sensor that is able to discriminate temperature and strain by calculating a cross coefficient matrix, as given by [21]

$$\begin{pmatrix} \Delta\varepsilon \\ \Delta T \end{pmatrix} = \begin{pmatrix} C_\varepsilon^1 & C_T^1 \\ C_\varepsilon^2 & C_T^2 \end{pmatrix}^{-1} \begin{pmatrix} \Delta\lambda_1 \\ \Delta\lambda_2 \end{pmatrix} = \begin{pmatrix} 2.4 & 144.7 \\ 0 & 88.7 \end{pmatrix}^{-1} \begin{pmatrix} \Delta\lambda_1 \\ \Delta\lambda_2 \end{pmatrix} \quad (7)$$

where $\Delta\varepsilon$ and ΔT are the variations of strain and temperature. C_ε^1, C_T^1 and C_ε^2, C_T^2 represent the strain and temperature coefficients of dip 1 and dip 2, respectively. $\Delta\lambda_1$ and $\Delta\lambda_2$ are the wavelength shift of dip 1 and dip 2, respectively.

To verify the accuracy of the cross coefficient matrix, a proof experiment has been implemented by generating different temperatures and strains to evaluate the performance of LPFGs sensor. The measurement results are shown in Table I. It indicates that the relative measurement error of the temperature sensing

is smaller than 2.5% and the relative error of the strain sensing is smaller than 5%. Therefore, the FMF-LPFGs turns out to be very promising for temperature and strain discriminative measurement

IV. Conclusion

In conclusion, thanks to the flexible, precise and repeatable fabrication technique that is enabled by femtosecond laser direct writing, long-period fiber grating in few-mode fiber was demonstrated in this work, and the properties of the FMF-LPFGs have been characterized thoroughly. The mode coupling mechanisms of the FMF-LPFGs are revealed by both the transmission spectrum and the mode patterns. In addition, the temperature, strain and twist responses of the resonance dips have been calibrated by experiments. By using the different responses to external temperature and strain, a cross coefficient matrix was established and dual-parameter discriminative measurement is achieved with less than 2.5% relative temperature measurement error and less than 5% relative strain measurement error. The results presented in this paper provide a theoretical and experimental reference for FMF-LPFGs fabrication based on femtosecond laser direct writing technique, and the fabricated devices show great potential for multi-parameter sensing in the future.

References

[1] R. Ryf *et al.*, "Mode-division multiplexing over 96 km of few-mode fiber using coherent 6 x 6 MIMO processing," *J. Lightw. Technol.,* vol. 30, no. 4, pp. 521–531, Feb. 2012, doi: 10.1109/jlt.2011.2174336.

[2] S. Ramachandran, Z. Wang, and M. Yan, "Bandwidth control of long-period grating-based mode converters in few-mode fibers," *Opt. Lett.,* vol. 27, no. 9, pp. 698–700, May 2002, doi: 10.1364/OL.27.000698.

[3] A. M. Vengsarkar, P. J. Lemaire, J. B. Judkins, V. Bhatia, T. Erdogan, and J. E. Sipe, "Long-period fiber gratings as band-rejection filters," *J. Lightw. Technol.,* vol. 14, no. 1, pp. 58–65, Jan. 1996, doi: 10.1109/50.476137.

[4] D. Davis, T. Gaylord, E. Glytsis, S. Kosinski, S. Mettler, and A. Vengsarkar, "Long-period fibre grating fabrication with focused CO_2 laser pulses," *Electron. Lett.,* vol. 34, no. 3, pp. 302–303, Feb. 1998, doi: 10.1049/el:19980239.

[5] I. Giles, A. Obeysekara, R. Chen, D. Giles, F. Poletti, and D. Richardson, "Fiber LPFG mode converters and mode selection technique for multimode SDM," *IEEE Photon. Technol. Lett.*, vol. 24, no. 21, pp. 1922–1925, Nov. 2012, doi: 10.1109/LPT.2012.2219044.

[6] B. Li *et al.*, "Long-period fiber gratings inscribed in few-mode fibers for discriminative determination," *Opt. Exp.,* vol. 27, no. 19, pp. 26307–26316, Sep. 2019, doi: 10.1364/OE.27.026307.

[7] Y. Zhu *et al.*, "Strain-insensitive and high-temperature long-period gratings inscribed in photonic crystal fiber," *Opt. Lett.,* vol. 30, no. 4, pp. 367–369, Feb. 2005, doi: 10.1364/OL.30.000367.

[8] G. Rego, "Annealing of arc-induced gratings at high temperatures," *Electron. Lett.,* vol. 45, no. 19, pp. 972–974, Sep. 2009, doi: 10.1049/el.2009.1767.

[9] J. He *et al.*, "Single-mode helical Bragg grating waveguide created in a multimode coreless fiber by femtosecond laser direct writing," *Photon. Res.,* vol. 9, no. 10, pp. 2052–2059, Oct. 2021, doi: 10.1364/prj.434719.

[10] Y. Kondo, K. Nouchi, T. Mitsuyu, M. Watanabe, P. G. Kazansky, and K. Hirao, "Fabrication of long-period fiber gratings by focused irradiation of infrared femtosecond laser pulses," *Opt. Lett.,* vol. 24, no. 10, pp. 646–648, May 1999, doi: 10.1364/OL.24.000646.

[11] M. Beresna, M. Gecevičius, and P. G. Kazansky, "Ultrafast laser direct writing and nanostructuring in transparent materials," *Adv. Opt. Photon.,* vol. 6, no. 3, pp. 293–339, Sep. 2014, doi: 10.1364/AOP.6.000293.

[12] M. Ams, G. D. Marshall, P. Dekker, J. A. Piper, and M. J. Withford, "Ultrafast laser written active devices," *Laser Photon. Rev.,* vol. 3, no. 6, pp. 535–544, Oct. 2009, doi: 10.1002/lpor.200810050.

[13] F. Chen and J. V. de Aldana, "Optical waveguides in crystalline dielectric materials produced by femtosecond-laser micromachining," *Laser Photon. Rev.,* vol. 8, no. 2, pp. 251–275, Mar. 2014, doi: 10.1002/lpor.201300025.

[14] J. Thomas, C. Voigtlaender, R. G. Becker, D. Richter, A. Tuennermann, and S. Nolte, "Femtosecond pulse written fiber gratings: A new avenue to integrated fiber technology," *Laser Photon. Rev.*, vol. 6, no. 6, pp. 709–723, Nov. 2012.

[15] K. Zhou, M. Dubov, C. Mou, L. Zhang, V. K. Mezentsev, and I. Bennion, "Line-by-line fiber Bragg grating made by femtosecond laser," *Photon. Technol. Lett.,* vol. 22, no. 16, pp. 1190–1192, Aug. 2010, doi: 10.1109/LPT.2010.2050877.

[16] Y. Zhao *et al.*, "Femtosecond laser inscribed axial long-period fiber gratings in two-mode fiber for efficient optical angular momentum generation," in *Proc. Opt. Fiber Commun. Conf.*, 2017, pp. 1–3.

[17] T. Erdogan, "Fiber grating spectra," *J. Lightw. Technol.,* vol. 15, no. 8, pp. 1277–1294, Aug. 1997, doi: 10.1109/50.618322.

[18] R. Slavík, "Coupling to circularly asymmetric modes via long-period gratings made in a standard straight fiber," *Opt. Commun.,* vol. 275, no. 1, pp. 90–93, Jul. 2007, doi: 10.1016/j.optcom.2007.02.064.

[19] X. Shu, L. Zhang, and I. Bennion, "Sensitivity characteristics of long-period fiber gratings," *J. Lightw. Technol.,* vol. 20, no. 2, pp. 255–266, Feb. 2002, doi: 10.1109/50.983240.

[20] Y. J. Rao, Y. P. Wang, Z. L. Ran, and T. Zhu, "Novel fiber-optic sensors based on long-period fiber gratings written by high-frequency CO_2 laser pulses," *J. Lightw. Technol.,* vol. 21, no. 5, pp. 1320–1327, May 2003, doi: 10.1109/jlt.2003.810561.

[21] R. Wang, M. Tang, S. Fu, Z. Feng, W. Tong, and D. Liu, "Spatially arrayed long period gratings in multicore fiber by programmable electrical arc discharge," *IEEE Photon. J.,* vol. 9, no. 1, Feb. 2017, Art. no. 4500310, doi: 10.1109/JPHOT.2016.2639499.